MODEL ATMOSPHERES AND QUANTITATIVE SPECTROSCOPY OF CENTRAL STARS OF PLANETARY NEBULAE*

R.P. Kudritzki[1] and R.H. Méndez[1,2]

[1]Institut für Astronomie und Astrophysik
 der Universität München
 Scheinerstr. 1, D-8000 München 80, Germany

[2]Instituto de Astronomia y Fisica del Espacio
 Buenos Aires, Argentina

1. INTRODUCTION

It is a good tradition in IAU Symposia about PN to have a paper on model atmospheres. However, this is always a difficult task for the authors, because the majority of the PN researchers still believe that the best model atmosphere for a Central Star is a black body. Of course, this puts a theorist in stellar atmospheres into a somewhat desperate position. However, Central Stars of Planetary Nebulae (here-after CSPN) - as all other stars - show spectral lines. And we will try to use the opportunity of this paper to convince that - as for all other stars - the quantitative analysis of these lines on basis of model atmospheres yields extremely valuable information about the physical nature of the stars.

   Modern quantitative spectroscopy of hot stars has two aspects: the analysis of spectral lines formed (i) in the hydrostatic photo-spheres and (ii) in the supersonically expanding winds. Both aspects will be covered by this paper.

2. SPECTROSCOPY OF PHOTOSPHERIC LINES

2.1. Analysis Method

The basis for the quantitative spectroscopic analysis of photospheric lines is given by NLTE model atmospheres (Kudritzki, 1973, 1976; Husfeld et al., 1984; Husfeld, 1986; Groth, 1986) and subsequent extensive NLTE multi-level line formation calculations for H, HeI and HeII (Kudritzki and Simon, 1978; Husfeld, 1986; Husfeld et al., 1987; Herrero, 1987a and b).

*Based on observations collected at the European Southern Observatory, La Silla, Chile

The principle of the analysis is as follows: For "cool" objects (T_{eff} < 50000K) the HeI/HeII ionization ratio determines the effective temperature, the wings of the Balmer lines yield the gravity and the absolute strengths of the HeII lines gives the helium abundance defined as the number fraction $y = N_{He}/(N_H+N_{He})$. For hotter objects (T_{eff} > 50000K) the HeI lines are too weak so that no helium ionization equilibrium can be used for the temperature determination. Instead, an alternative method is applied which makes use of the fact that at these hot temperatures the profile shapes of H and HeII lines contain information about both: T_{eff} and log g. (A detailed description of this method is given by Méndez et al., 1981 and Méndez et al., 1983). In this way T_{eff} and log g can be derived simultaneously from the shapes of the H and HeII profiles, whereas y follows again directly from the absolute strength of the HeII lines.

It is of course clear that these methods require excellent spectra, i.e. well defined profile shapes of high S/N (>50) taken with (almost) linear detectors. A particular problem of CSPN is the contamination of photospheric lines with nebular emission lines. This requires in addition a rather high spectral resolution of $\lambda/\Delta\lambda$ > 10^4. Since CSPN are generally faint, this is not an easy goal. However, the present day Cassegrain-Echelle spectrographs with CCD detectors (as the ESO CASPEC) are ideally suited for this purpose (see also paper by McCarthy, this meeting). These instruments form the basis for modern quantitative spectroscopy of CSPN.

In addition to excellent spectra a <u>high quality NLTE line-formation theory</u> is needed to extract the information about the stellar parameters. Since the pioneering developments by Auer and Mihalas (1972) and the later slight improvements by Kudritzki (1976) and Kudritzki and Simon (1978), no substantial progress was made for some time. However, recently, the consequent use of the Auer-Heasley-method (Auer and Heasley, 1976) in the NLTE code DETAIL (developed by J. Giddings, 1980) allowed a significant improvement in the detailed treatment of the transition schemes of the model atoms in question.

One of the major disadvantages of the old NLTE line formation calculations was the neglect of Stark broadening in the line profiles when solving rate equations and radiative transfer simultaneously. Stark broadening was only taken into account in the final formal solution after the iteration cycle for the occupation numbers was finished. As pointed out by Méndez et al. (1983) this approximation might affect the cores of the computed hydrogen and helium lines. Herrero (1987 a and b) using the new numerical technique of "Accelerated Lambda Iteration" by Werner and Husfeld (1985) has now overcome this approximation and treated this problem correctly. He included Stark broadening in the rate equations, added a large number of radiative transitions and took also into account the line overlap of H and HeII by treating both atoms simultaneously. As a result he obtained significantly deeper line cores, which led to much better agreement with the observations. (Examples are given in Fig. 1 and 2). As an important consequence of this result some CSPN effective temperatures obtained spectroscopically by Méndez et al. (1981, 1983, 1985) had to be revised towards 10 to 20 percent higher values.
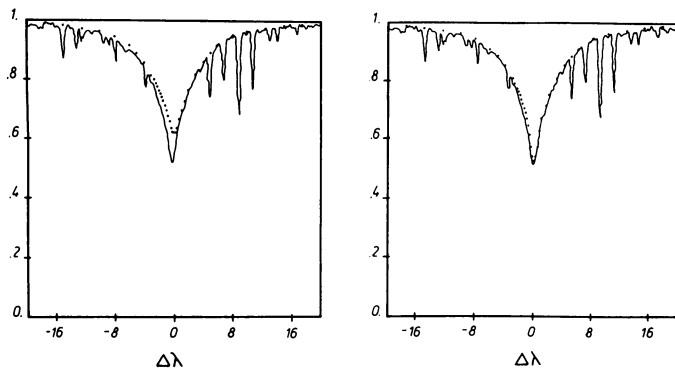
Fig. 1: Observed high S/N Hγ-profile of the O9.5V star τ Sco compared with standard NLTE calculations (left) and the recent improvements by Herrero, 1987a (right).
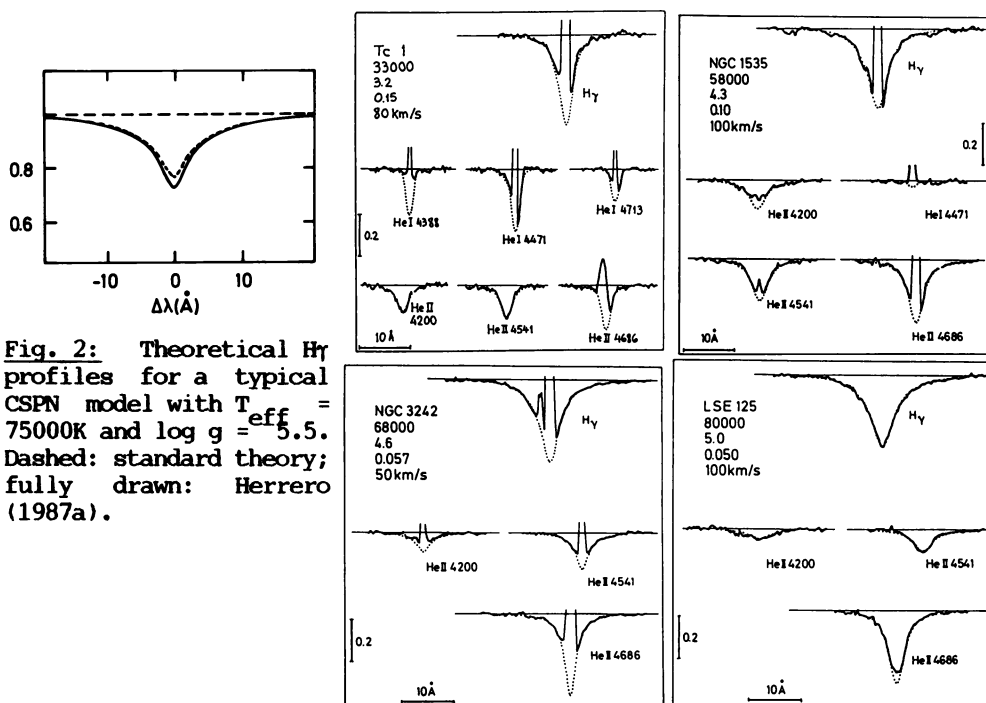
Fig. 2: Theoretical Hγ profiles for a typical CSPN model with T_{eff} = 75000K and log g = 5.5. Dashed: standard theory; fully drawn: Herrero (1987a).

Fig. 3: 4 examples of the profile fits obtained by Méndez et al.(1987). For every object T_{eff}, log g, y and the rotational (or macroturbulent) velocity (obtained from metal lines) are given.

2.2. Application to high resolution, high S/N optical spectra of CSPN

The analysis methods outlined in the preceding section have now very recently been applied on a large sample of CSPN observed with high resolution and high S/N (Méndez et al., 1987). The observational material consists of ESO 3.6 m CASPEC plus CCD spectra. The covered wavelength range is 4000 to 5000 Å, the resolution 0.2 to 0.3 Å. A S/N of 50 to 100 was achieved in most cases. The limiting magnitude is m_v = 14. 26 CSPN were observed in this way including for the first time objects embedded in nebulae with high surface brightness, which were omitted in the previous studies (Méndez et al., 1981, 1983, 1985).

The estimated uncertainties are ±10% in T_{eff}, ±0.2 in log g and ±20% in y. These estimates include probable systematic errors, which will be discussed below.

Table 1: Spectroscopic parameters of CSPN

	$T_{eff}(10^3 K)$	log g	y	$M(M_\odot)$	d(kpc)
NGC 7293	90±10	6.9±.2	.009±.005	.55±.02	0.30
LSE 125	78±5	5.0±.2	.05±.02	.60±.03	1.3
NGC 7009	75±10	4.7±.2	.05±.03	.70±.05	2.5
NGC 4361	75±5	5.4±.2	.05±.02	.55±.01	1.3
NGC 1360	72±5	5.3±.2	.07±.02	.55±.01	0.67
NGC 3242	68±5	4.6±.2	.05±.02	.65±.04	2.0
NGC 1535	58±5	4.3±.2	.09±.02	.66±.04	2.7
IC 2448	55±5	4.5±.2	.11±.02	.57±.02	4.5
NGC 6891	50±8	3.9±.2	.07±.02	.75±.07	3.8
NGC 2392	47±7	3.6±.2	.35±.10	.90±.13	2.7
NGC 6629	47±5	3.8±.2	.08±.02	.73±.06	2.4
IC 4637	47±5	3.9±.2	.09±.02	.67±.04	1.6
EGB 5	42±5	5.8±.2	.003±.002	?	?
IC 418	36±4	3.3±.2	.15±.04	.77±.07	2.0
He 2-182	36±2	3.4±.15	.09±.02	.70±.05	7.4
He 2-108	33±2	3.1±.2	.15±.03	.81±.09	8.3
Tc 1	33±2	3.2±.15	.14±.02	.72±.06	3.8
M 1-26	33±2	3.2±.15	.12±.02	.72±.06	1.9
H 2-1	33±2	3.3±.15	.08±.02	.67±.04	4.6
He 2-138	27±2	2.7±.2	.30±.10	.87±.12	5.0
He 2-162	27±2	2.9±.15	.18±.03	.68±.04	4.0
He 2-151	25±2	2.7±.15	.12±.02	.73±.06	8.0

Fig. 3 displays typical profile fits, which give an impression about the quality of the spectra and the theory applied: Tc1 is a typical example of the cooler objects, where nebular emission affects only H and HeI. (The emission of HeII 4686 comes from the stellar wind, see below). It is evident that without high resolution the HeI absorptions would be undetectable. Typical nebular contamination is

also important for the hotter objects NGC 1535 and 3242. Note that NGC 3242 is the prototype of the "continuous spectral type", which according to Kudritzki et al. (1981 a and b) has no real physical meaning. It reflects simply a resolution problem in the case of narrow photospheric lines and very strong nebular lines. LSE 125 is a good example of an object within a low surface brightness nebula, which allows to fit also the very cores of the lines.

The spectroscopic parameters obtained by Méndez et al. (1987) are summarized in Table 1, which also contains already stellar masses and distances. How these quantities are derived is discussed in the two following sections.

2.3. Evolution of CSPN

The model atmosphere approach yields (besides the helium abundance) T_{eff} and log g of the CSPN. This enables us to test the predictions of stellar evolution theory in a completely alternative observational way, namely the log g, log T_{eff}-diagram. This approach has a fundamental advantage: It is independent on any assumption about nebular distances and therefore allows us to constrain the evolution of CSPN in an observationally independent way.

Fig. 4 shows the log g, log T_{eff}-diagram of 22 CSPN. From the transformation of post AGB evolutionary tracks into this diagram the evolutionary status of the CSPN is evident: They are clearly post-AGB objects with masses between 0.55 and 0.9 $M_\odot$, which nicely agrees with the masses of DA White Dwarfs (Weidemann and Koester, 1984). Since the error box arising from the fit of the observed hydrogen and helium lines just by chance has the same inclination as the tracks, a rather precise determination of individual masses is possible from Fig. 4. These masses are given in Table 1.

A few comments are necessary. First, the sample is clearly biased by the selection of more luminous (i.e. more massive) CSPN in this first pioneering step. Future observations using the ESO EFOSC spectrograph will allow to complete the sample in view of mass distribution statistics. Second, the masses of the objects close to the Eddington limit have larger uncertainties for two reasons: In the log g, log T_{eff}-plane the constant luminosity tracks of higher masses lie closer, which for the same Δlog g $\approx$ ±0.2 yields $\Delta M \approx$ ±0.13 $M_\odot$ for an object like NGC 2392, whereas $\Delta M \approx$ ±0.03 $M_\odot$ for the objects of $M/M_\odot \approx$ 0.6. Moreover, as will be demonstrated below, photospheric geometrical extension and contamination of photospheric profiles by stellar wind emission become a problem close to the Eddington limit. This might additionally affect the analysis of an extreme object like NGC 2392.

Fig. 4 contains one CSPN, which is obviously not a post AGB-object: EGB 5. This object is located in that part of the diagram, which is normally restricted to subluminous O-stars not surrounded by a nebula (for a recent review, see Kudritzki, 1987). The evolutionary status of EGB 5 is not clear. An attractive possibility might be close binary evolution. The helium poor sdO-star LB 3459 = AA Dor (see Kudritzki et al., 1982) might be an example of such a case. Fig. 5 demonstrates that the Balmer lines of EGB 5 are significantly broader

278
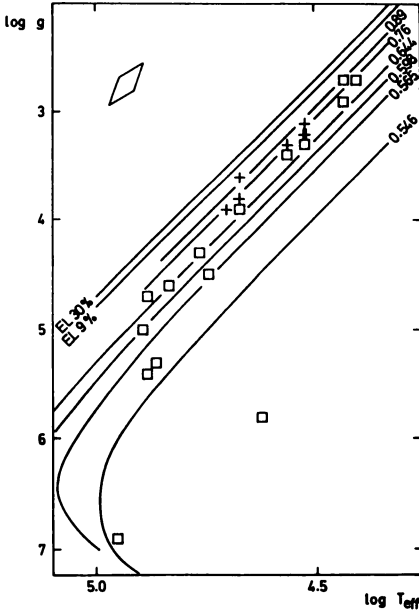
Fig. 4: The log g, log T$_{eff}$ diagram of 22 CSPN. Crosses refer to Of-type objects, whereas squares hold for spectral type O. A typical error box is given in the upper left. Post AGB evolutionary tracks (Wood and Faulkner, 1986; Schönberner, 1983) have been transformed into this diagram and are labelled by their mass in solar units. The Eddington limits for y=0.09 and 0.3 are also shown (from Méndez et al., 1987).
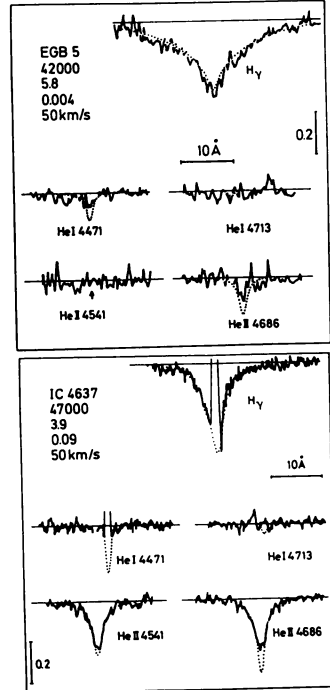
Fig. 5: Profiles of EGB 5 and IC 4637 demonstrating the high gravity of EGB 5.
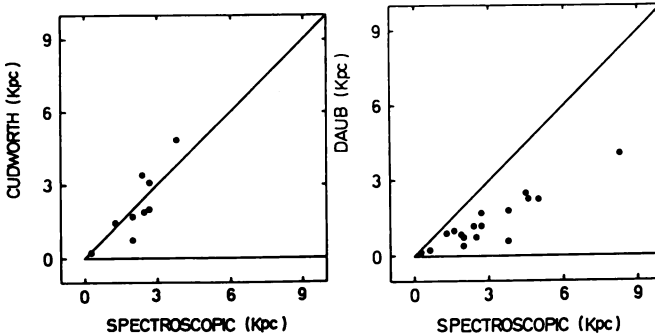
Fig. 6: PN distances by Daub (1982) and Cudworth (1974) vs. spectroscopic distances.
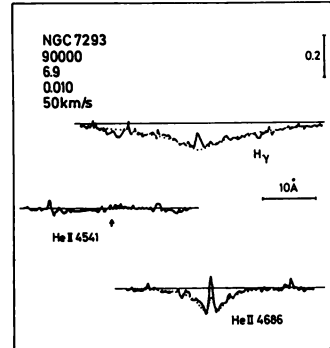
Fig. 10: Profile fit of NGC 7293.

than for IC 4637, a typical post-AGB CSPN of similar T_{eff}. Thus, the high gravity of EGB 5 provides some uncertainty for the evolutionary scenario of CSPN. Obviously not every CSPN went through the AGB channel. The question is, how many of this type do exist. This will be subject to future spectroscopic programs.

2.4. Spectroscopic distances

The model atmosphere approach allows also to obtain distances. From the log g-log T_{eff} diagram and post AGB tracks, masses can be derived. Using the gravity this yields stellar radii. On the other hand, the comparison of observed (dereddened) flux with the stellar surface flux predicted by the final model atmosphere for every individual object yields angular diameters. These combined with the radii give the "spectroscopic distances". The typical individual uncertainty of this procedure is 25%.

The spectroscopic distances are also given in Table 1. A comparison of these values with other frequently cited statistical distances (Cahn and Kaler, 1971; Daub, 1982) reveals that they are much larger. On the other hand, we find agreement with Seaton (1966) and Cudworth (1974) (see Fig. 6). We note that by the increased distances the most luminous PN in the sample of Méndez et al. (1987) become as luminous as the most luminous PN in the Magellanic Clouds, removing in this way a pronounced lack of bright "nearby" galactic PN (see Jacoby, 1980, 1983). The spectroscopic distances are also confirmed by Barlow (this meeting) in his study of LMC and SMC PN.

## 2.5. A test of the reliability of the model atmosphere approach

An ideal test of the reliability of the model atmosphere approach is its application on faint blue stars in globular clusters. Heber and Kudritzki (1986) have recently performed such a test for the sdO-star ROB 162 in the globular cluster NGC 6397. ROB 162 is the only known hot blue sdO star in this metal poor (Fe/H = -2) cluster. Fig. 7 shows the result of the high resolution (again ESO CASPEC spectra with S/N ≈ 50) spectroscopy of this rather faint (m_v = 13.3) object. As stellar parameters T_{eff} = 51000±2000K, log g = 4.5±0.2 and y = 0.09±0.02 were obtained.

It is now possible to determine M, R and L of ROB 162 in two alternative ways. First the spectroscopic method using the log g, log T_{eff}-diagram and second using the known cluster distance of d = 2400 pc (Alcaino and Liller, 1980), which combined with T_{eff} gives the radius directly and which combined with log g yields also the mass. The results of the two methods are compared in table 2, which shows remarkable agreement.
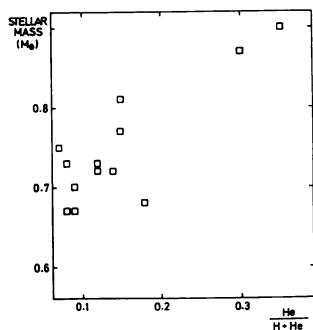
If we use the spectroscopically determined radius together with T_{eff}, then the comparison of observed and model calculated flux yields d = 2560 pc, which agrees well with the value mentioned above, which was obtained by main sequence and horizontal branch fitting.
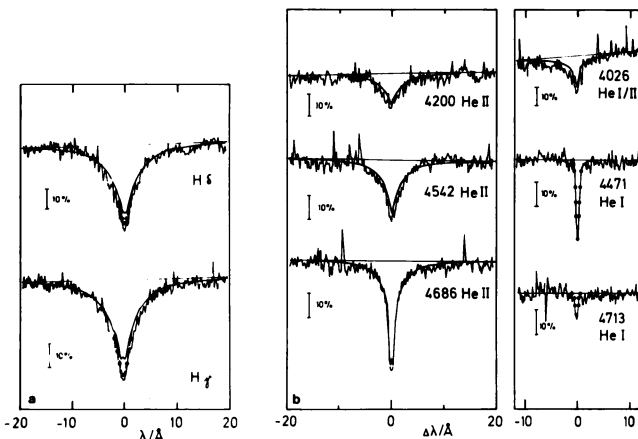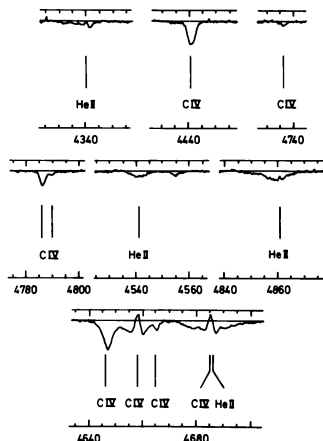
Fig. 7: Profile fits obtained in the NLTE analysis of ROB 162 (from Kudritzki and Heber, 1986).
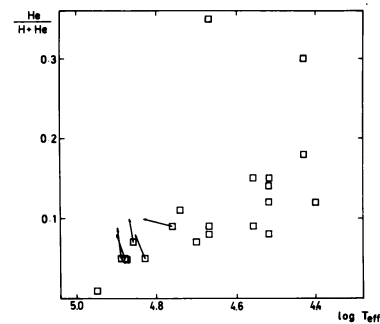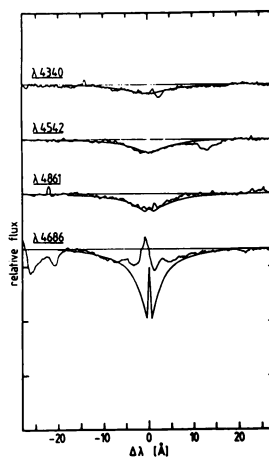

Fig. 8: Helium number fraction of CSPN as function of T_{eff}. The arrows indicate corrections applied to the results by Méndez et al. (1987), if the new broadening theory by Schöning and Butler (1988, in prep. for A&A) for HeII 4686 is used.

Fig. 11: ESO 3.6 m CAS-PEC line profiles of NGC 246. Note the enormous strength of the CIV lines and the absence of hydrogen.

Fig. 12: Profile fits of NGC 246 (from Husfeld, 1986).

Fig. 9: Stellar mass versus helium number fraction. The diagram is restricted to objects with log T_{eff} < 4.8.

Table 2: M,R,L of ROB 162 by two alternative methods

	spectroscopic method	cluster distance method
$R/R_\odot$	$0.70^{+0.18}_{-0.14}$	0.66 ± 0.04
$M/M_\odot$	$0.56^{+0.04}_{-0.02}$	$0.50^{+0.3}_{-0.2}$
$\log L/L_\odot$	3.5 ± 0.2	3.4 ± 0.1

2.6. Photospheric abundances

<u>2.6.1. Helium.</u> In Figs. 8 and 9 the helium abundances of Table 1 are plotted as function of T_{eff} or $M/M_\odot$ respectively. The arrows in Fig. 8 indicate shifts, which have to be applied to Table 1, if the new broadening theory for HeII 4686 by Schöning and Butler (1988, in prep. for A&A) is used. Note that all stars have been checked by us for this effect. However, only those marked by the arrows are significantly affected, since they exhibit strong absorption wings of HeII 4686. Since $M/M_\odot$ and distance d are also slightly affected we give a correction table to Table 1.

Table 3: New parameters due to new HeII 4686 broadening theory

object	T_{eff}	log g	y	$M/M_\odot$	d(kpc)
LSE 125	85000	5.1	0.09	0.62	1.2
NGC 7009	82000	4.8	0.08	0.72	2.4
4361	82000	5.5	0.09	0.55	1.2
1360	80000	5.4	0.09	0.55	0.63
3242	75000	4.7	0.09	0.68	2.0
1535	70000	4.6	0.11	0.67	2.1
IC 2448	65000	4.8	0.13	0.58	3.5
4637	50000	4.0	0.09	0.68	1.5

From Fig. 8 it is evident that, as long as the CSPN evolution proceeds with constant luminosity, the helium abundances are larger or equal than the solar value of y=0.09. That means that in this stage the abundances obviously reflect AGB-abundances.

Fig. 9 on the other hand indicates for these objects a trend of higher helium abundances being correlated with higher post-AGB masses of our CSPN. This could be the result of stronger mass-loss or dredge up at the AGB.

The situation changes completely after the CSPN have turned down on the WD cooling sequence: The low helium abundance object at highest $\log T_{eff}$ in Fig. 8 is NGC 7293, our only high gravity object (log g ≈

7) in Fig. 4. Fig. 10 shows the profile fit for this object demonstrating the reliability of the stellar parameters, in particular the value of y=0.01 ≈ 0.1 $y_\odot$. Obviously, the process of gravitational settling, which leads to the cooling sequence of helium poor DA stars, sets in immediately after the CSPN have curved around from constant luminosity to the cooling track.

2.6.2. Photospheric metallicity. The determination of photospheric metal abundances in hot stars by means of non-LTE methods is now possible if high quality optical and UV spectra can be used for the analysis. Very detailed and improved non-LTE multi-level calculations are now available for the following ions: C II,III,IV; N II,III,IV,V; O II,IV; Mg II, Ca II; Al III, Si II,III,IV. This has been done very recently at the Munich observatory by Keith Butler, Dirk Husfeld, Sylvia Becker and Franziska Eber. This work has already been successfully applied on Population I OB-stars (Kudritzki et al., 1987a; Becker and Butler, 1987; Schönberner et al., 1988) and OB subdwarfs (Husfeld et al., 1987; Kudritzki, 1987). At this meeting a first attempt for two cooler CSPN of the Méndez et al. (1987) sample is presented by Roth et al. In our opinion, the detailed investigation of photospheric metal abundances will be one of the very interesting directions of future quantitative CSPN spectroscopy.

2.7. The extreme helium rich CSPN of NGC 246

It is well known since the work of Aller (1948) and Heap (1975) that NGC 246 is a peculiar CSPN with evidently no trace of hydrogen in its photosphere. Interestingly, the nebular abundances appear to be quite normal (Heap, 1975). Fig. 11 shows part of the ESO 3.6 m CASPEC spectra (S/N ≈ 100) of this star. Dirk Husfeld (1986) has analysed this object as part of his thesis at Munich observatory. The results of his work are given in Table 4. Fig. 12 displays the corresponding profile fits.

Table 4: Parameters of the central star of NGC 246

T_{eff}	130000±15000 K	$\dfrac{n_{He}}{n_{He}+n_H+n_C}$	: 50 to 90%
log g	$5.7^{+0.4}_{-0.2}$		
$M/M_\odot$	0.7	$\dfrac{n_C}{n_{He}+n_H+n_C}$	: 10 to 50%
$\dfrac{n_H}{n_{He}+n_H+n_C}$	< 10%		

NGC 246 is obviously the hottest CSPN studied by quantitative spectro-

scopy so far. Besides the absence of hydrogen it is characterized by an enormous amount of carbon in its photosphere. According to Husfeld (1986) we are looking at an extreme case of AGB mass-loss, which left the AGB intershell matter as the present photosphere.

At this point we want to stress that extreme helium rich CSPN are not rare. According to Méndez et al. (1986) 35% of all spectroscopically well studied CSPN belong to this class!

2.8. Problems

2.8.1. Systematic errors due to present NLTE-models for CSPN. The NLTE
models used by Méndez et al. are still far from being physically perfect. They make use of a variety of approximations of which the most important ones are now discussed here.
- metal line blanketing is neglected:
  The inclusion of NLTE metal line blanketing was for a long time impossible for simple numerical reasons. On the other hand, LTE blanketed models are completely unreliable at these high temperatures. However, after the work by Anderson (1985), Werner and Husfeld (1985) and Werner (1986) methods are known which will allow the computation of realistic NLTE line blanketing very soon. In fact Werner (1987) in his thesis has already calculated CSPN models, which include the blanketing of more than 100 lines of H, He and C in NLTE. The effect on the temperature structure is surprisingly low in the region of formation of optical H and He lines. Thus, we expect corrections of T_{eff} only by up to 5 to 10% by this effect.
- wind blanketing is neglected:
  Wind blanketing is induced by the backscattering of photospheric photons due to the metal lines formed in the surrounding stellar wind envelope. Abbott and Hummer (1985) and Bohannan et al. (1986) have investigated this effect in the case of the 04f-star ζ Puppis. A $\Delta T_{eff} \approx 4000K$ was found. For CSPN a similar estimate is not so easy as it requires accurate knowledge of the mass-loss rates, which is observationally not available at the moment. However, following the results of radiation driven wind theory as presented in the second part of this paper, we would expect significant effects with respect to T_{eff} for objects with $M/M_{\odot} > 0.75$. On the other hand, since the correction in T_{eff} would proceed along the inclined error bars of Fig. 4, conclusions with respect to stellar mass would be less affected.
- atmospheric extension is neglected:
  The NLTE models are planeparallel, which means that spherical extension is neglected. This approximation was investigated by Gruschinske and Kudritzki (1979) for extended hydrostatic NLTE models for sdO and CSPN. Only small effects were found. However, for the extreme objects like NGC 2392 and some other cooler low gravity objects close to the Eddington limit systematic changes in the line profiles might be important. In these cases also the effects of stellar winds causing probably deviations from the hydrostatic equilibrium might be important. This effect will also be discussed below.

2.8.2. The Zanstra discrepancy. One of the longstanding problems of CSPN is the discrepancy between the Zanstra temperatures derived from nebular hydrogen and ionized helium lines and the spectroscopic effective temperature. Husfeld et al. (1984) indicated a way out for hot CSPN close to the Eddington limit. Henry and Shipman (1986) suggested a solution for CSPN which have a lower helium abundance due to gravitational settling. With the well defined stellar parameters of Table 1 it is possible to reinvestigate this problem. For this purpose we defined "Zanstra ratios" ZR in the following way:

$$ZR = \log \frac{\text{Number of ionizing photons } (cm^{-2}s^{-1})}{\text{stellar continuum flux at 5480A } (erg \ cm^{-2}s^{-1} \ Hz^{-1})}$$

In the next step we investigated whether our NLTE models for the final T_{eff}, log g, y are able to reproduce the observed Zanstra ratios. This is done in Fig. 13 for black bodies as well as NLTE models.

It is obvious that for both blackbodies and NLTE models a deficiency of hydrogen Lyman photons is observed. However, this is not an enormous factor, which could easily be explained by the neglect of metal line blanketing or by the fact that the nebulae are optically thin. For the HeII photons we observe a clearly pronounced excess relative to the NLTE models. Using blackbodies the effect is smaller but still present.

From Fig. 13 we conclude that the hydrostatic planeparallel NLTE models generally fail to produce the observed stellar flux shortward of the HeII edge at 228A at least for the sample of Table 1. This casts some doubts on the reliability of the models. However, we will suggest a solution at the end of the paper.

3. SPECTROSCOPY OF STELLAR WIND LINES

3.1. Observation of winds in CSPN spectra

After the advent of the IUE satellite it became undoubtedly clear that stellar winds are present in many CPN (Heap, 1978; Perinotto, 1982). P-Cygni profiles in the UV have been detected for a variety of objects and many attempts have been made to determine terminal velocities v_∞ as well as mass-loss rates $\dot{M}$. A typical example is the Central star of NGC 3242 (see Fig. 14). Here the detailed fit of the observed NV P-Cygni profile yielded v_∞ = 2200±100 km/s and log $\dot{M}$ = -9.0±1.0 ($\dot{M}$ in $M_\odot$/yr). The large error in $\dot{M}$ reflect mainly the uncertainty of the ionization calculations, which to our eyes is typical for these objects. The general situation is best described in the paper by Cerruti-Sola and Perinotto (1985) and by Perinotto (invited paper, this meeting).

For the purpose of stellar atmosphere theory including stellar winds it is important to have a reliable hypothesis for the wind driving mechanism. Thus the question is, whether these winds are radiation driven as in the case of massive OB-stars. We present two observational arguments:
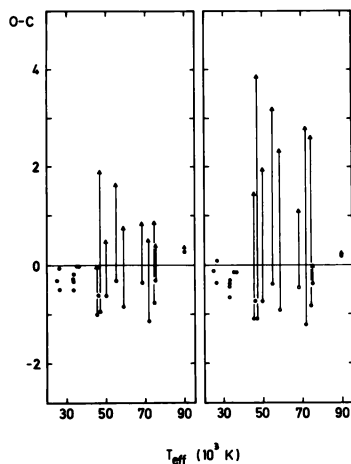
Fig. 13: Observed minus computed Zanstra ratios for H (open circles) and HeII (triangles) as function of stellar effective temperature of Table 1. The left part uses black bodies for the stellar flux, the right part the final NLTE models of Table 1.
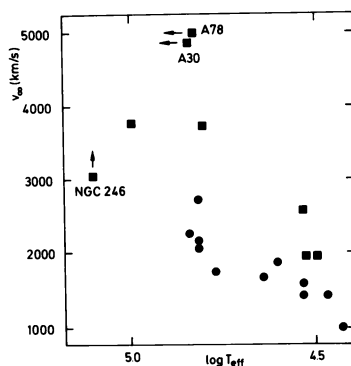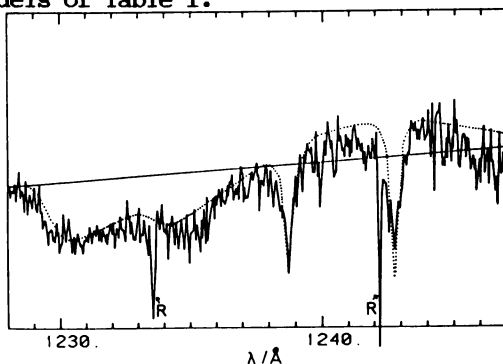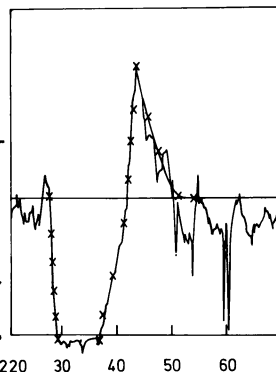

Fig. 14: IUE high resolution profile of the NV P-Cygni profile of NGC 3242. The dotted curve shows the theoretical profile fit obtained by detailed comoving frame calculations (from Hamann, Kudritzki, Méndez, Pottasch, 1984).

Fig. 16: Terminal velocity versus T_{eff} for CSPN. Squares are H-deficient objects; circles, normal Hydrogen abundance.

Fig. 17: NV λ 1240 IUE high resolution profile of ζ Puppis compared with prediction of a selfconsistent radiation driven wind model (crosses), which has only the stellar parameters T_{eff}, log g, R as free parameters (from J. Puls, 1987).
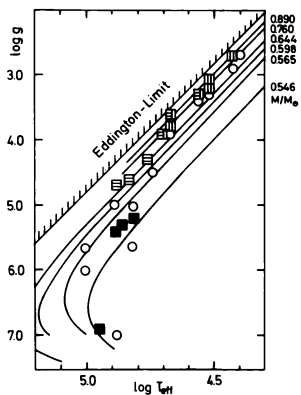
Fig. 15: The (log g, log T_{eff})-diagram of CPN according to Méndez et al. (1987, 1985). Evolutionary tracks (labelled by $M/M_{\odot}$) are also shown. IUE wind detections are indicated by ▤. Wind detections by optical spectra (HeII 4686 in emission <=> Of-spectral type) are given by ▥. Definitely no winds (IUE plus optical) is coded by ■. Objects with no winds in the optical but no IUE high resolution information yet available are described by o. The Eddington-limit is also indicated.

- The stellar wind features observable in the UV and/or optical become stronger for CSPN closer to the Eddington limit. This is demonstrated clearly by Fig. 15.
- The terminal velocity v_∞ of CSPN winds increases with T_{eff} (see Fig. 16). This strongly points to radiation driven winds being present in the outer layers of CSPN, since in this case the terminal velocity increases with the surface escape velocity. CSPN evolve at constant luminosity towards the blue, so that the escape velocity increases. Consequently we expect the terminal velocity to increase with T_{eff}.

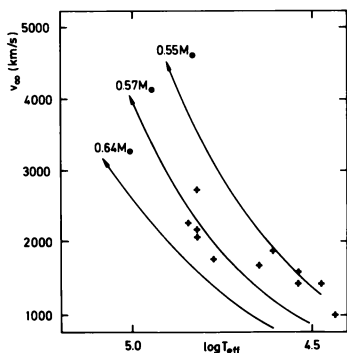## 3.2. Radiation driven wind models for CSPN

Motivated by the results of Fig. 15 and 16 we have calculated radiation driven wind models along the evolutionary tracks of post-AGB objects (Schönberner, 1983; Wood and Faulkner, 1986) of different masses (see Fig. 4). These calculations include the following significant improvements relative to the original wind theory by Castor, Abbott and Klein (1975):
- improved dynamics by dropping the radial streaming approximation (see Pauldrach et al., 1986; Kudritzki et al., 1987b). These improvements allowed to match the observed values of terminal velocity and mass loss rate for a variety of massive OB stars, including P Cygni.
- detailed multi-level NLTE calculations for ionization and excitation (Pauldrach, 1987). They include, simultaneously with hydrodynamics, the self-consistent treatment for 10000 line transitions of 133 ions of 26 elements, electron collisions and continuum radiative transfer. For the calculation of the line force, 100000 lines in NLTE were considered.
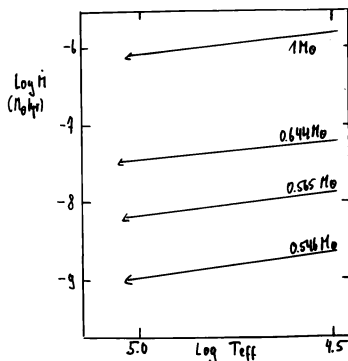
These calculations solved for massive O-stars the "superionization" problem: they produce NV and OVI for cool winds with a wind temperature similar to T_{eff} (see Fig. 17). The self-consistent treatment of multiple scattering, as developed by Puls (1987), has not yet been included. This will be done in a refined step of the calculations.

Fig. 18 shows the calculated relation between terminal velocity and T_{eff} along the evolutionary tracks, including the observed values for CSPN. The result is extremely convincing. It allows to read off stellar masses directly, and suggests that the masses of CSPN are in a rather narrow range between 0.5 and 0.8 solar masses (Schönberner, 1981; Méndez et al., 1985, 1987). This reveals the power of stellar wind models for the determination of stellar masses. (Note, however that Fig. 18 contains different CSPN as Table 1. Thus, the difference in mass distribution is not necessarily alarming).
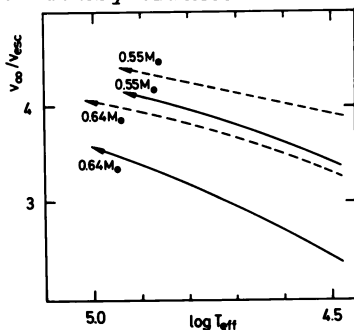
Fig. 19 shows the development of theoretical mass-loss rates along the tracks. The theory predicts very strong mass-loss rates for $M > 0.65\ M_\odot$, when the objects come closer to the Eddington limit. This might have consequences for evolutionary time scales and nebular dynamics. In the latter case it is interesting to note that wind momentum ($\dot{M} v_\infty$) and energy ($\dot{M} v_\infty^2$) input into the nebula increase during the CSPN evolution!
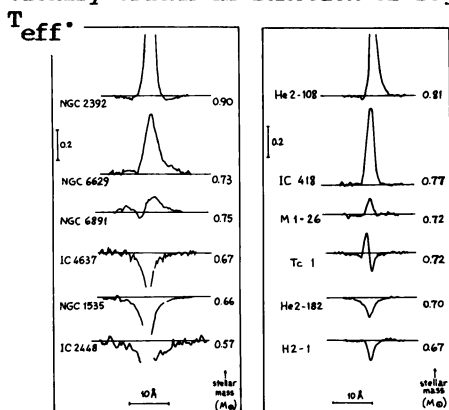
Fig. 18: Same as Figure 16 for CSPN with normal H abundance, but including wind calculations along evolutionary tracks.
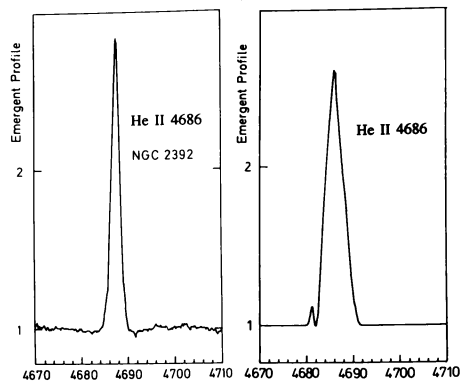

Fig. 20: The ratio v_∞/v_{esc} vs. T_{eff} for (--) hydrogen deficient objects and (-) objects containing mainly hydrogen.

Fig. 24: The observed HeII 4686 emission of NGC 2392 (left) compared with a corresponding model calculation (right).

Fig. 19: Logarithm of mass-loss rate predicted by radiation driven wind theory along the evolutionary tracks as function of log T_{eff}.

Fig. 21: The behaviour of the stellar HeII 4686 as a function of the stellar mass. The left and the right panels are for objects with T_{eff} around 50000K and 35000K, respectively.
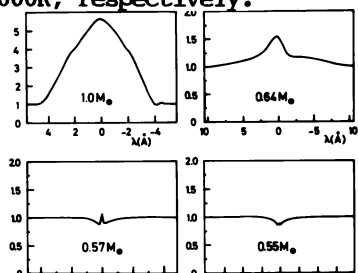
Fig. 23: As Fig. 22 but HeII 4686. Note the enormous emission at one solar mass.

3.3. Wind distances

For massive OB-stars the relation $v_\infty = 3\, v_{esc}$ is observed, as long as $T_{eff} > 30000K$ (Abbott, 1978, 1982). Kaler et al. (1985) adopted this relation for CSPN also and combined it with the core-mass luminosity relation $R_\star^2\, T_{eff}^4 = f(M/M_\odot)$. Since $v_{esc}^2 = 2\,G\,M(1-\Gamma)/R_\star$ (with $\Gamma = L_\star/L$), one can determine in this way the CSPN mass and radius and therefore the distance, as soon as T_{eff} is known. Kaler et al. used this method to derive "wind distances" for CPN. The crucial question is, however, whether $v_\infty = 3\, v_{esc}$ holds in general for CPN. Fig. 20 shows that this is not the case. Our calculations predict that the ratio v_∞/v_{esc} depends on stellar mass, evolutionary status, photospheric helium abundance, etc. Consequently, the method of wind distances - although intrinsically very powerful - will need some refinements to become finally quantitatively reliable.

3.4. Stellar winds in the optical spectra of CSPN

As already discussed, the high resolution optical spectroscopy of CSPN by Méndez et al. shows clearly that stellar wind emission line features are systematically more strongly pronounced for objects which are located closer to the Eddington limit. A convincing example is given by the behaviour of HeII 4686 as displayed in Fig. 21. It is important to test, whether radiation driven wind models can reproduce this behaviour.

For this purpose, a new type of "unified model atmospheres" has been developed at the Munich Observatory by R. Gabler (1986) and A. Wagner (1986) in cooperation with J. Puls, A. Pauldrach and R.P. Kudritzki. These NLTE model atmospheres are spherically extended, in radiative equilibrium, and include the density and velocity distribution of radiation driven winds. The spectra of H and He lines are then calculated for these models by detailed NLTE multi-level calculations in the whole atmosphere, thus treating the contribution of subsonic deeper and supersonic outer layers to the emergent line profile in the correct self-consistent unified way, including Stark-effect broadening and velocity fields. We have calculated a sequence of such models for $T_{eff} = 50000K$ and stellar masses equal to 0.55, 0.57, 0.64, 0.75, 0.85 and 1 solar masses. The corresponding luminosities for the CSPN (or the gravities or the radii) were obtained from the evolutionary tracks mentioned already in the previous section.

By these calculations it was intended to investigate four important questions:
- Are the strategic lines used by Méndez et al. for photospheric analysis contaminated by wind emission or absorption?
  Fig. 22 demonstrates that this is not the case as long as $M < 0.8\, M_\odot$.
- Do typical optical wind lines increase, when approaching the Eddington-limit as demonstrated by Fig. 21?
  Fig. 23 shows that in fact the new models can reproduce this behaviour at least qualitatively. Fig. 24 displays the most extreme example: NGC 2392.
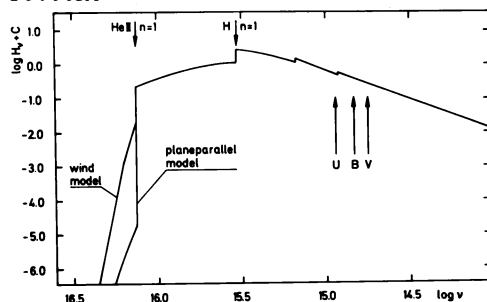- Does spherical extension together with wind outflow affect the shape
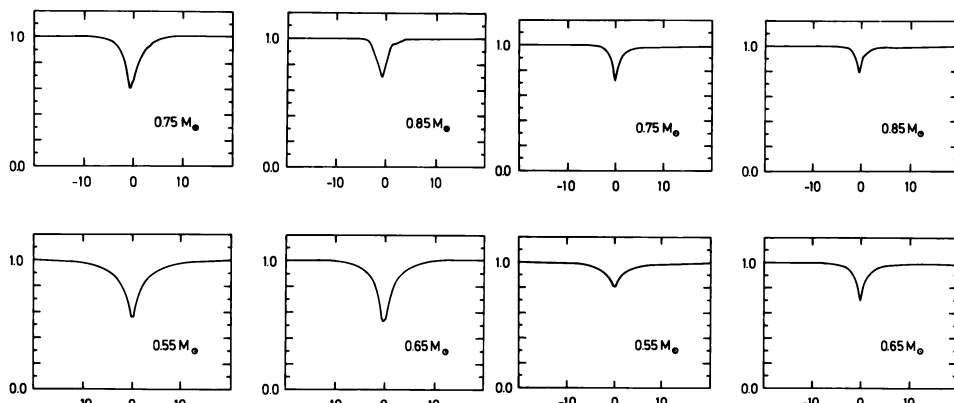
Fig. 22: Hγ (left) and HeII 4542 (right) profiles for unified NLTE models of different mass at T_{eff} = 50000K.
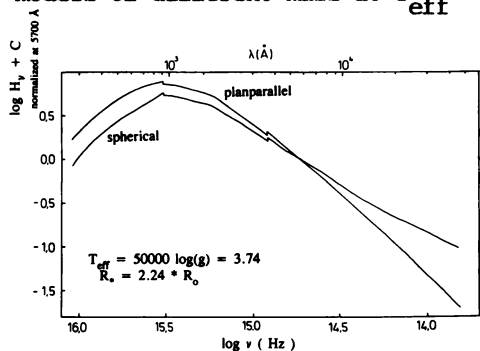
Fig. 25: Effects of spherical extension on the observable energy distribution for a 1 M$_\odot$ model.

Fig. 26: The effects of the wind velocity field on emergent energy distribution for λ < 228Å in the extended model compared with hydrostatic planeparallel case for M = 0.55 M$_\odot$.
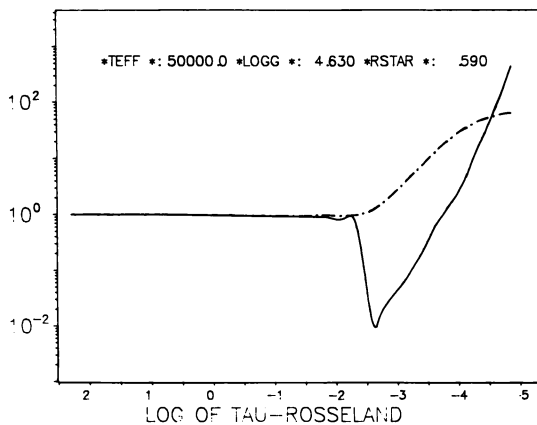
Fig. 27: The departure coefficient of the HeII ground state as function of logarithm of Rosseland optical depth for a hydrostatic planeparallel model (dashed-dotted) and the extended model including the wind.

of the observable energy distribution?
No significant differences between the planeparallel and new unified
models were found for 1000Å $\leq \lambda \leq$ 10000Å as long as M $\leq$ 0.8 M$_\odot$. Fig.
25, however, demonstrates a significant effect for M = 1 M$_\odot$. This
flattening of the energy distribution is observed for NGC 2392 (see
paper by Heap and Torres, this meeting).
- Do stellar winds affect the continuum formation of HeII photons ($\lambda \leq$
228Å)?
The answer is: yes, dramatically. Fig. 26 shows the comparison for
0.55 M$_\odot$, i.e. a model away from the Eddington-limit with a weak
wind. The extended model including winds yields about 10^3 HeII-
photons more than the classical hydrostatic, planeparallel model!
The physical reason is as follows: Because of its enormous optical
thickness the HeII-continuum is formed in the outermost layers,
where the mass-ouflow is clearly supersonic. Thus hydrostatic models
are in this case invalid for the formation of the HeII-continuum! In
the model including the wind the very high optical thickness of the
HeII resonance lines is reduced by the presence of the supersonic
velocity field. This enables the strong continuum longward of 228Å
to pump, by the HeII resonance transition, electrons into the n=2
stage, from which further ionization takes place. This leads to a
depopulation of the ground state just in the region, where the
continuum shortward of 228Å becomes optically thin (Fig. 27). As a
result the usual strong HeII-absorption edge is significantly de-
creased, as shown in Fig. 26.
This effect will need further quantitative investigation. It looks,
however, very promising to overcome the problem displayed in Fig. 13!

4. CONCLUSIONS

The modern quantitative spectroscopy of CSPN has reached a stage,
where stellar parameters can be determined with high precision. Not
only effective temperature, gravity and helium abundance but also mass
and distance are obtained from the photospheric spectroscopy. Stellar
wind lines quantitatively analysed using the improved theory of radia-
tion driven winds allow - at least in principle - an independent
determination of mass, radius and distance. Abundance determinations
in CSPN photospheres and winds are at hand. A precise determination of
mass-loss rates from UV lines (NV, CIV, SiIV etc.) and optical lines
(Hα, HeII 4686) will be possible by means of strongly improved multi-
level NLTE calculations in the winds of CSPN. Thus in total an immense
potential for quantitative spectral analysis has been developed during
the recent years. The future work will be characterized by the use of
this potential.

REFERENCES

Abbott, D.C.: 1978, Astrophys. J. 225, 893
Abbott, D.C.: 1982, Astrophys. J. 259, 282
Abbott, D.C., Hummer, D.G.: 1985, Astrophys. J. 294, 286
Alcaino, G., Liller, W.: 1980, Astron. J. 85, 680
Aller, L.H.: 1948, Astrophys. J. 108, 462
Anderson, L.S.: 1985, Astrophys. J. 298, 848
Auer, L.H., Mihalas, D.: 1972, Astrophys. J. Suppl. 24, 193
Auer, L.H., Heasley, J.N.: 1976, Astrophys. J. 205, 165
Becker, S., Butler, K.: 1987, Astron. Astrophys. submitted
Bohannan, B., Abbott, D.C., Voels, S.A., Hummer, D.G.: 1986, Astrophys. J. 308, 728
Cahn, J.H., Kaler, J.B.: 1971, Astrophys. J. Suppl. 22, 319
Castor, J., Abbott, D.C., Klein, R.: 1975, Astrophys. J. 195, 157
Cerruti-Sola, M., Perinotto, M.: 1985, Astrophys. J. 291, 237
Cudworth, K.M.: 1974, Astron. J. 79, 1384
Daub, C.T.: 1982, Astrophys. J. 260, 612
Gabler, R.: 1986, Diplomarbeit, Universität München
Giddings, J.: 1980, thesis, University College London
Groth, H.G.: 1986, unpublished work
Gruschinske, J., Kudritzki, R.P.: 1979, Astron. Astrophys. 77, 341
Hamann, W.R., Kudritzki, R.P., Méndez, R.H., Pottasch, S.R.: 1984, Astron. Astrophys. 139, 459
Heap, S.R.: 1975, Astrophys. J. 196, 195
Heap, S.R.: 1978, IAU Symp. 83, p. 99
Heber, U., Kudritzki, R.P.: 1986, Astron. Astrophys. 169, 244
Henry, R.B.C., Shipman, H.L: 1986, Astrophys. J. 311, 774
Herrero, A.: 1987a, Astron. Astrophys. 171, 189
Herrero, A.: 1987b, Astron. Astrophys., in press
Husfeld, D.: 1986, Ph.D. Thesis, Universität München
Husfeld, D., Butler, K., Heber, U., Drilling, J.: 1987, Astron. Astrophys., submitted
Husfeld, D., Kudritzki, R.P., Simon, K.P., Clegg, R.: 1984, Astron. Astrophys. 134, 139
Jacoby, G.H.: 1980, Astrophys. J. Suppl. 42, 1
Jacoby, G.H.: 1983, IAU Symp. 103, p. 427
Kaler, J.B., Mo, J.E., Pottasch, S.R.: 1985, Astrophys. J. 288, 305
Kudritzki, R.P.: 1973, Astron. Astrophys. 28, 108
Kudritzki, R.P.: 1976, Astron. Astrophys. 52, 11
Kudritzki, R.P.: 1987, "Spectroscopic Constraints on the Evolution of Subluminous O-stars and Central Stars of PN", Proc. of IAU Coll. No. 95 on Faint Blue Stars, ed. Davis Philip, in press
Kudritzki, R.P., Groth, H.G., Butler, K., Husfeld, D., Becker, S., Eber, F., Fitzpatrick, E.: 1987a, Proc. ESO Workshop on SN 1987A", ed. I.J. Danziger, p. 39

Kudritzki, R.P., Méndez, R.H., Simon, K.P.: 1981a, Astron. Astrophys. 99, L15

Kudritzki, R.P., Méndez, R.H., Simon, K.P.: 1981b, ESO Messenger 26, 7

Kudritzki, R.P., Pauldrach, A., Puls, J.: 1987b, Astron. Astrophys. 173, 293

Kudritzki, R.P., Simon, K.P.: 1978, Astron. Astrophys. 70, 653

Kudritzki, R.P., Simon, K.P., Lynas-Gray, A.E., Kilkenny, D., Hill, P.W.: 1982, Astron. Astrophys. 106, 254

Méndez, R.H., Kudritzki, R.P., Gruschinske, J., Simon, K.P.: 1981, Astron. Astrophys. 101, 323

Méndez, R.H., Kudritzki, R.P., Herrero, A., Husfeld, D., Groth, H.G.: 1987, Astron. Astrophys., in press

Méndez, R.H., Kudritzki, R.P., Simon, K.P.: 1983, IAU Symp. 103, p. 343

Méndez, R.H., Kudritzki, R.P., Simon, K.P.: 1985, Astron. Astrophys. 142, 289

Méndez, R.H., Miguel, C.H., Heber, U., Kudritzki, R.P.: 1986, in IAU Colloquium 87 "Hydrogen deficient stars and related objects", ed. K. Hunger et al., Reidel, Astrophys. Sp. Sci. Library 128, p. 323

Pauldrach, A.: 1987, Astron. Astrophys. 183, 295

Pauldrach, A., Puls, J., Kudritzki, R.P.: 1986, Astron. Astrophys. 164, 86

Perinotto, M.: 1982, IAU Symp. 103, p. 323

Puls, J.: 1987, Astron. Astrophys. 184, 227

Schönberner, D.: 1981, Astron. Astrophys. 103, 119

Schönberner, D.: 1983, Astrophys. J. 272, 708

Schönberner, D., Herrero, A., Becker, S., Butler, K., Kudritzki, R.P., Simon, K.P.: 1988, Astron. Astrophys., in press

Seaton, M.: 1966, MNRAS 132, 113

Wagner, A.: 1986, Diplomarbeit, Universität München

Weidemann, V., Koester, D.: 1984, Astron. Astrophys. 132, 195

Werner, K.: 1986, Astron. Astrophys. 161, 177

Werner, K.: 1987, thesis, University of Kiel

Werner, K., Husfeld, D.: 1985, Astron. Astrophys. 148, 417

Wood, P.R., Faulkner, D.J.: 1986, Astrophys. J. 307, 659